CHALMERS | UNIVERSITY OF GOTHENBURG

A linear nonconforming finite element method for Maxwell's equations in two dimensions

PETER HANSBO
THOMAS RYLANDER

A linear nonconforming finite element method for Maxwell's equations in two dimensions

Peter Hansbo, Thomas Rylander

A linear nonconforming finite element method for Maxwell's equations in two dimensions

Peter Hansbo, [a]   Thomas Rylander [b]

[a]*Department of Mathematical Sciences, Chalmers University of Technology and University of Gothenburg, SE–41296 Göteborg, Sweden*

[b]*Department of Signals and Systems, Chalmers University of Technology, SE–41296 Göteborg, Sweden*

Abstract

We suggest a linear non-conforming triangular element for Maxwell's equations and test it in the context of the vector Helmholtz equation for the electric field. The element uses discontinuous normal fields and tangential fields with continuity at the midpoint of the element sides, an approximation related to the Crouzeix-Raviart element for Stokes. The element is stabilized using the jump of the tangential fields, giving us a free parameter to decide. We give dispersion relations for different stability parameters and give some numerical examples, where the results converge quadratically with the mesh size for problems with smooth boundaries. The proposed element is free from spurious solutions and, for cavity eigenvalue problems, the eigenfrequencies that correspond to well-resolved eigenmodes are reproduced with the correct multiplicity.

Key words: Maxwell's equations, stabilized methods, finite element, interior penalty method, non-conforming method.

1   Introduction

The electric field solution to Maxwell's equations resides in $H(\mathrm{curl})$ and it requires tangential continuity. Imposing H^1-continuity on the approximation of the electric field usually leads to pollution of the spectrum, i.e. unphysical non-zero eigenvalues that mix with the lowest physical eigenvalues. In such a situation, modes that should have zero eigenvalues (corresponding to gradient fields) in the continuous setting have non-zero eigenvalues in the discrete setting. This has led to the introduction of vector elements [17,18] that are tailor-made for approximation in $H(\mathrm{curl})$ and they have become very popular for numerical simulations in electromagnetics, cf. Monk [15]. For such elements

of the lowest order, the degrees of freedom are associated with the edges of the element and therefore they are often referred to as edge elements.

The triangular edge elements suffer in that the corresponding mass matrix cannot be lumped (with positive entries in the mass matrix) unless an angle condition is fulfilled [12], or other non-standard measures are taken [14,10]. In general, the standard edge elements thus require implicit time stepping. On the other hand, curl-conforming approximations on rectangles and bricks do allow for mass-lumping and explicit time-stepping, cf. Cohen [7]. For example, the lowest order curl-conforming approximation on rectangles and bricks can be lumped by means of trapezoidal integration, and its analogue finite difference scheme was introduced by Yee [24]. Thus, it is often referred to as the Yee scheme but it is probably more well-known as the finite-difference time-domain (FDTD) scheme [21], which emphasizes its typical usage for electrodynamic problems. For the purpose of boundary modelling, the Yee scheme has to be coupled to other methods. It is feasible to couple implicitly time-stepped tetrahedrons (or triangles) with the Yee scheme in time domain methods, cf. Degerfelt and Rylander [9]. For the purpose of explicit schemes on unstructured meshes, Discontinuous Galerkin (DG) methods can be formulated on simplicial meshes [4]. These have been explored in the setting of time-harmonic problems [19] and eigenvalue problems [22]. They do allow for mass lumping and explicit time-stepping on unstructured simplicial meshes, cf. Hesthaven and Warburton [13]; however, DG methods achieve mass lumping at the cost of extra degrees of freedom at the inter-element boundaries—a solution that becomes particularly expensive for the low-order approximations that are popular for engineering applications.

In this paper, we propose a new nonconforming element for the approximation of the curl-conforming electric field of Maxwell's equations in two dimensions. Our element yields a diagonal mass matrix and thus explicit time-stepping can be used on arbitrary unstructured meshes. The element represents linear field variations exactly and it has degrees of freedom associated with the edges of the element, where the normal field component is discontinuous and the tangential field component is continuous at the midpoint of each edge. Consequently, we achieve a significant reduction in the number of degrees of freedom as compared to the corresponding DG method without sacrificing the ability to perform explicit time-stepping. We demonstrate that our new element yields very accurate approximations on a grid of equilateral triangles. In particular, we use this type of discretization in the homogeneous bulk of the computational domain, and revert to an unstructured mesh of body-conforming triangles in the vicinity of curved boundaries. The proposed element is also a good candidate for coupling the Yee scheme on rectangles to a boundary-fitted triangular mesh, a highly desirable quality for fast and accurate simulations.

2

2 Problem formulation and finite element method

We consider Maxwell's double curl eigenvalue problem in two somewhat different situations: (i) plane wave propagation in free space for a given wave number $\boldsymbol{k}$ which gives the numerical dispersion relation $\omega(\boldsymbol{k})$ of the proposed element; and (ii) a cavity resonator that is defined by the bounded domain Ω with perfect electrically conducting boundary $\partial\Omega$ and outward pointing normal $\boldsymbol{n}$. Thus, we wish to find the electric field $\boldsymbol{E}$ and frequency ω such that

$$\nabla \times \nabla \times \boldsymbol{E} - \left(\frac{\omega}{c_0}\right)^2 \boldsymbol{E} = 0 \quad \text{in } \Omega, \tag{1}$$

with (i) $\Omega = \mathbb{R}^2$ for the dispersion analysis and (ii) a bounded domain Ω with $\boldsymbol{n} \times \boldsymbol{E} = 0$ on $\partial\Omega$ for the cavity resonator problem.

For the presentation of the new element, we focus on the cavity resonator problem and postpone further discussions on the dispersion analysis to Section 3. For the cavity resonator problem stated in weak form, we seek

$$\boldsymbol{E} \in V := \{\boldsymbol{v} \in H(\mathrm{curl}; \Omega) : \boldsymbol{v} \times \boldsymbol{n} = 0 \text{ on } \partial\Omega\}$$

such that

$$\int_\Omega (\nabla \times \boldsymbol{E})(\nabla \times \boldsymbol{v})\, d\Omega - \left(\frac{\omega}{c_0}\right)^2 \int_\Omega \boldsymbol{E} \cdot \boldsymbol{v}\, d\Omega = 0 \tag{2}$$

for all $\boldsymbol{v} \in V$. Here

$$H(\mathrm{curl}; \Omega) := \{\boldsymbol{v} : \boldsymbol{v} \in L_2(\Omega) \text{ and } \nabla \times \boldsymbol{v} \in L_2(\Omega)\}.$$

In order to discretize this problem, we let $\mathcal{T}_h$ denote a triangulation of Ω into simplices T of diameter h_T, and let $\mathcal{E}_h$ denote the set of edges E, of length h_E, in $\mathcal{T}_h$. We then define the following nonconforming finite element space:

$$V^h := \{\, \boldsymbol{v} \in [L_2(\Omega)]^2 : \boldsymbol{v} \in [P^1(T)]^2 \; \forall T \in \mathcal{T}_h, \; \boldsymbol{n} \times \boldsymbol{v} \text{ is continuous at}$$
$$\text{the midpoints of all interior edges, and } \boldsymbol{n} \times \boldsymbol{v} = 0 \text{ at the}$$
$$\text{midpoints of all edges along } \partial\Omega\}.$$

We note that this space is related to the classical Crouzeix–Raviart (CR) space [8], but with edge midpoint continuity enforced only for the tangential component. The standard CR element is known not to converge for the Maxwell double curl problem, cf. Brenner, Li, and Sung [2] (where instead an element-wise divergence free version of the CR element was analyzed and shown to converge). Additionally, a version of the CR element using only tangential degrees of freedom was analyzed by Monk and Parrot [16] and shown to give erroneous dispersion relations.

Denoting the jump of the tangential component of $\boldsymbol{v} \in V^h$ across edges by $[\![\boldsymbol{n} \times \boldsymbol{v}]\!]$, with $[\![\boldsymbol{n} \times \boldsymbol{v}]\!] = \boldsymbol{n} \times \boldsymbol{v}$ if the edge is on $\partial\Omega$, where $\boldsymbol{n}$ is a normal to the edge E, our finite element method is to find $(\boldsymbol{E}^h, \omega^2) \in V^h \times \mathbb{R}$ such that

$$a_h(\boldsymbol{E}^h, \boldsymbol{v}) - \left(\frac{\omega}{c_0}\right)^2 (\boldsymbol{E}^h, \boldsymbol{v}) = 0 \quad \forall \boldsymbol{v} \in V^h, \tag{3}$$

where

$$a_h(\boldsymbol{u}, \boldsymbol{v}) := \int_\Omega (\nabla_h \times \boldsymbol{u})\,(\nabla_h \times \boldsymbol{v})\,d\Omega + \sum_{E \in \mathcal{E}_h} \int_E \frac{\gamma}{h_E} [\![\boldsymbol{n} \times \boldsymbol{u}]\!]\,[\![\boldsymbol{n} \times \boldsymbol{v}]\!]\,ds \tag{4}$$

and

$$(\boldsymbol{u}, \boldsymbol{v}) := \int_\Omega \boldsymbol{u} \cdot \boldsymbol{v}\,d\Omega.$$

Here, $\nabla_h \times$ denotes the element-wise application of the curl operator and γ is a user specified penalty parameter. We note that the tangential jumps have been added to the equation in the same manner as in a DG method in order to increase stability of our numerical scheme. Computational experience shows that this term (with $\gamma > 0$) is indeed necessary; the piecewise $H(\mathrm{curl}; \Omega)$–norm is too weak to control the jumps (cf. also [3]). We also note that the DG scheme has two additional terms compared to (3); the bilinear form for DG can be written

$$a_h^{\mathrm{DG}}(\boldsymbol{u}, \boldsymbol{v}) = a_h(\boldsymbol{u}, \boldsymbol{v}) - \sum_{E \in \mathcal{E}_h} \int_E ([\![\boldsymbol{n} \times \boldsymbol{u}]\!]\,\{\nabla_h \times \boldsymbol{v}\} + [\![\boldsymbol{n} \times \boldsymbol{v}]\!]\,\{\nabla_h \times \boldsymbol{u}\})\,ds,$$

where $\{\cdot\}$ denotes a mean value of the indicated quantity across the edge E. These are consistency terms necessary to retain Galerkin orthogonality, yielding a best approximation result underlying optimal convergence properties. For our approximation, these terms are zero since $\nabla_h \times \boldsymbol{v}$ is piecewise constant and the mean value of $[\![\boldsymbol{n} \times \boldsymbol{v}]\!]$ is zero for all $\boldsymbol{v} \in V^h$. Thus our method is (weakly) consistent in the same sense as a standard DG method (the idea of retaining the stabilization terms for Crouzeix–Raviart was first used in another context in [11]).

In the theoretical framework for the analysis of DG approximations of the Maxwell eigenproblem presented by Buffa and Perugia [5], a key ingredient in the analysis is the use of an interpolant onto the corresponding edge element space. Due to the large size of the DG basis, the edge elements constitute a subset thereof, a fact that can be used in the analysis. One may view our method as a way of reducing the number of unknowns in the DG method without losing the property that the edge element basis is a subset of V^h: the linear edge element has full tangential continuity and a complete linear approximation inside the elements, cf. [18]. This space, with two degrees of freedom per edge, constitutes a subset of V^h with its three degrees of freedom per (interior) edge (a subset obtained as $\gamma \to \infty$). Note that this is not the

case for the standard Crouzeix–Raviart basis with its additional mean normal continuity.

The null space of our element is identical to that of the linear edge element in the limit $\gamma \to \infty$. For finite values of γ, the proposed element allows the tangential component of the vector field to be discontinuous except at the midpoint of each edge in the mesh, which clearly yields a larger space than that of the linear edge element. However, the null space of our discrete operator remains the same as the null space of the linear edge element also for γ finite. To see this, note that our formulation requires that modes that belong to the null space of the bilinear form (4) (with $\gamma > 0$) satisfy two conditions: (i) element-wise application of the curl operator is zero; and (ii) tangential continuity at element boundaries. Now, any discrete function that does not have zero tangential jump will give a contribution to $a_h(\cdot, \cdot)$. Thus, the null space of $a_h(\cdot, \cdot)$ is composed by those discrete functions that are linear on each element and have full tangential continuity; these are indeed the functions constituting the null space of the edge element. We also remark that numerical experience shows that choosing too small a γ does not have the effect of introducing singular spurious eigenvalues into the spectrum but rather increases tangential wiggling in the whole of the spectrum. This effect will also disappear under mesh refinement. Reasonable choices for γ are given in Section 3.

Some advantages of our approach compared to the linear edge element are:

- We have a free parameter γ with respect to which the scheme can be tuned (this will be discussed in the numerical examples below).
- Mass lumping is inherent.
- We have only one tangential degree of freedom per edge, which fits well with Yee's finite difference method.

Our approximation shares with the linear edge element the properties of

- having a full polynomial basis, which is beneficial with respect to accuracy in case of the Maxwell source problem with sources that feature non-zero divergence;
- not being divergence-free, which is beneficial in case of varying material (permittivity) parameters.

Finally, we remark that an alternative, computationally more advantageous, implementation of the element would be to follow Burman and Hansbo [6] and replace

$$\int_E \frac{\gamma}{h_E} [\![\boldsymbol{n} \times \boldsymbol{u}]\!] [\![\boldsymbol{n} \times \boldsymbol{v}]\!] \, ds$$

by

$$\int_E \gamma^* h_E [\![\boldsymbol{t} \cdot (\boldsymbol{t} \cdot \nabla \boldsymbol{u})]\!] [\![\boldsymbol{t} \cdot (\boldsymbol{t} \cdot \nabla \boldsymbol{v})]\!] \, ds$$

where $\boldsymbol{t}$ is a unit vector tangential to the edge and $\gamma^* > 0$ is a stabilization parameter (different from γ). This gives the same stability (cf. Lemma 9 in [6] for the basic argument) but requires only one Gauss–point per edge to integrate exactly.

3   Numerical tests

We test the proposed element on three different problems: (i) dispersion analysis based on plane wave propagation in free space; (ii) a cavity resonator problem with regular field solutions; (iii) a cavity resonator problem that features a sharp corner which supports field singularities. In the following, we evaluated the stabilization term in the bilinear form (4) by means of trapezoidal integration.

3.1   Dispersion analysis

We use a plane wave on the form $\boldsymbol{E} = \boldsymbol{E}_0 \exp[i(\omega t - \boldsymbol{k} \cdot \boldsymbol{x})]$ to compute the numerical dispersion relation on a period grid, cf. Monk and Parrot [16]. The periodic grid exploits a rhombic unit cell that is repeated in order to discretize $\mathbb{R}^2$. The unit cell is divided into two triangles, which makes it feasible to formulate an eigenvalue problem with nine degrees of freedom given the proposed element. We solve the eigenvalue problem in terms of its eigenmodes and the corresponding eigenvalues ω^2, where the frequency ω is a function of a prescribed wavevector $\boldsymbol{k}$. The analytically computed dispersion relation yields three possible solutions: $\omega = c_0 k$; $\omega = 0$; and $\omega = -c_0 k$.

As pointed out previously, the proposed method does not suffer from spurious modes, i.e. problems of the type that fields that vary on the scale of the grid yield frequencies in the same range as modes that are well-resolved by the grid. In the case of $\gamma > 0$, four of the branches correspond to conservative (gradient field) solutions with $\omega = 0$. One of these zero eigenvalues is associated with the node of the unit cell, where the continuous linear Lagrangian basis function ϕ_i has its degree of freedom. The remaining three zero eigenvalues are associated with edge-bubble basis functions that coincide with the three edges of the unit cell, where the potential is given by $\phi_i \phi_j$ and the indices i and j denote the end nodes of an edge in the unit cell. The lowest non-zero branch $\omega(\boldsymbol{k})$ models the physical dispersion relation, and in the following we present numerical results that assess its accuracy. The remaining four branches yield very high numerical frequencies that do not mix with the physical dispersion relation, and therefore can easily be identified and disregarded. (If the stabilization is removed by setting $\gamma = 0$, we have two zero eigenmodes associated with each

edge of the unit cell, i.e. in total seven zero branches.)

Let $||\cdot||_{k_{\max}}$ denote the L_1-norm evaluated on the disc shaped region $k \leq k_{\max}$. Figure 1 shows the relative error $||\omega_{\mathrm{n}} - \omega_{\mathrm{a}}||_{k_{\max}}/||\omega_{\mathrm{a}}||_{k_{\max}}$ as a function of the parameter γ for a grid of equilateral triangles characterized by the edge length h_E: (i) $h_E k_{\max}/\pi = 0.3$ – dashed curve; (ii) $h_E k_{\max}/\pi = 0.5$ – solid curve; and (iii) $h_E k_{\max}/\pi = 0.7$ – dash-dotted curve. Here, ω_{a} is the analytical frequency and ω_{n} is the corresponding numerical value. Thus, it is feasible to reduce the relative error to very low levels for the equilateral triangle, should the parameter γ be given an appropriate value. Shape deviations from the equilateral triangle that are on the order of percent do not change the optimal value of γ significantly and, in addition, the average error in the dispersion relation is rather unaffected by such perturbations. Since our objective is to find an element that combines explicit time-stepping with an accurate dispersion relation, we focus in the following on the case of equilateral triangles. Thus, we intend to use the equilateral triangles in the homogeneous bulk of the computational domain and other element shapes only in the vicinity of oblique and curved boundaries, where we wish to have a body-conforming mesh.
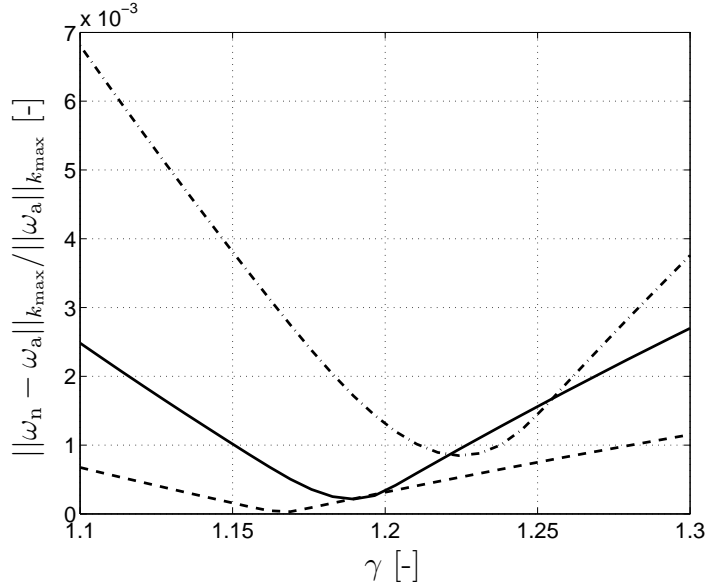
Fig. 1. The relative error $||\omega_{\mathrm{n}}-\omega_{\mathrm{a}}||_{k_{\max}}/||\omega_{\mathrm{a}}||_{k_{\max}}$ on the disc shaped region $k \leq k_{\max}$ as a function of the parameter γ for a grid of equilateral triangles: $h_E k_{\max}/\pi = 0.3$ – dashed curve; $h_E k_{\max}/\pi = 0.5$ – solid curve; and $h_E k_{\max}/\pi = 0.7$ – dash-dotted curve.

Figure 2 shows the pointwise relative error $|\omega_{\mathrm{n}} - \omega_{\mathrm{a}}|/\omega_{\mathrm{a}}$ as a function of the wavevector $\boldsymbol{k}$, given the optimized $\gamma = 1.19$ for the region $h_E k/\pi \leq 0.5$. It is clear that the relative error in the frequency is very low for a large region in $\boldsymbol{k}$-space. This makes it feasible to formulate an explicit time-stepping scheme that is accurate for broad frequency-band analysis, which also can be applied to rather large computational domains. We also note that the relative error in

7

the dispersion relation is proportional to $(h_E k)^2$ in the domain of asymptotic convergence, which is confined to the region $h_E k/\pi \lesssim 0.2$.
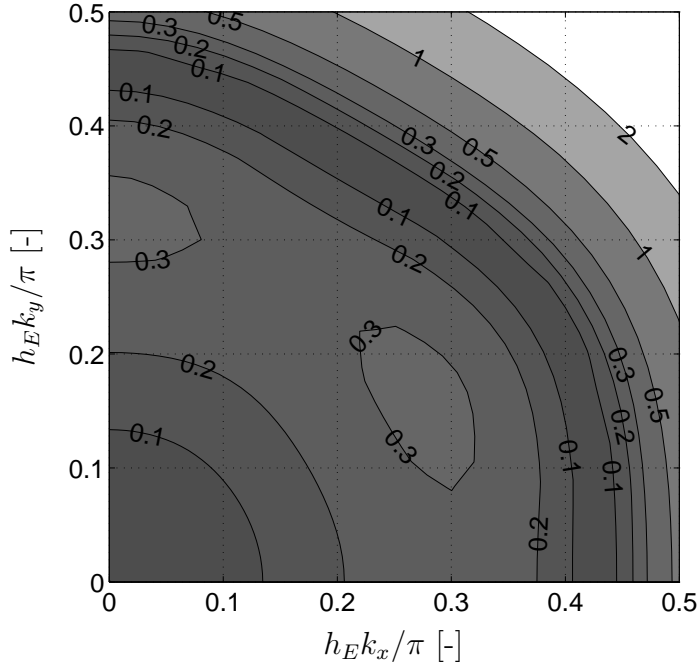
Fig. 2. The relative error $|\omega_\mathrm{n} - \omega_\mathrm{a}|/\omega_\mathrm{a}$ in per mille as a function of $\boldsymbol{k}$ for a grid of equilateral triangles of edge length h_E with $\gamma = 1.19$.

3.2 Cavity analysis

Next, we consider the eigenvalue problem (1) on a bounded region Ω, where we use the boundary condition $\boldsymbol{n} \times \boldsymbol{E} = 0$ on the boundary $\partial\Omega$. In all the tests that follow, the proposed element reproduces the lowest eigenvalues accurately with the correct multiplicity given that the corresponding eigenmodes are well-resolved. Moreover, the null space of the $\nabla \times \nabla\times$-operator is preserved. Let the number of internal nodes be denoted by n_in, the number of internal edges by n_ie and the number of edges on the external boundary by n_be. We find that $\gamma = 0$ yields a null space of dimension $n_\mathrm{in} + 2n_\mathrm{ie} + n_\mathrm{be}$. When stabilization is applied to all edges on the boundary of and internal to the computational domain, the dimension of the null space reduces to $n_\mathrm{in} + n_\mathrm{ie}$. This result is in agreement with our analysis of the null space associated with the $\nabla \times \nabla\times$-operator.

In the following, we compare the accuracy and performance of the proposed element with the lowest order edge element [17] in two different settings: (i) triangular elements; and (ii) rectangular elements with mass lumping by means of trapezoidal integration. (Note that the lumped rectangular edge element is

8

equivalent [20] to the spatial discretization used by the FDTD scheme [21].)
For comparisons in terms of accuracy, we consider the convergence of the low-
est eigenvalue on a uniformly refined mesh of unstructured triangles. Moreover,
we attempt to assess the performance of the proposed element, which appears
to be most competitive on grids of equilateral triangles due to its low errors
in the dispersion relation if an optimized value of γ is used. Therefore, we
use meshes of the type shown in Fig. 3 for performance estimates. It con-
sists of a structured grid of equilateral triangles in the homogeneous bulk of
the computational domain in combination with a layer of unstructured trian-
gles close to the boundary, which allows for a body-conforming discretization.
Consequently, we cannot expect strictly uniform convergence for these meshes
although we use uniform and hierarchic refinement for the equilateral triangles
in the bulk. However, we note that the thickness of the layer of unstructured
elements is proportional to mesh size and it is assumed that the unstructured
body-fitted mesh yields a negligible contribution to the global error for suffi-
ciently high resolutions.
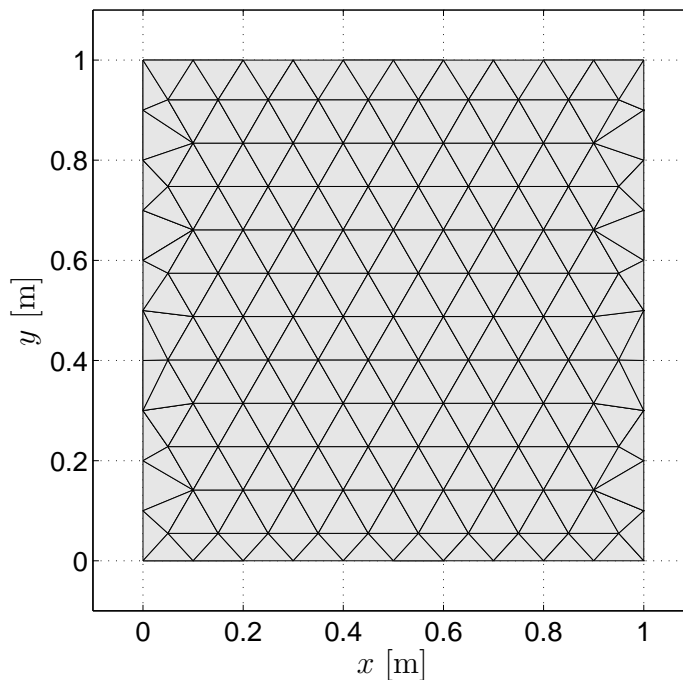
Fig. 3. Triangulation of square cavity that consists of two regions: (i) a structured
grid of equilateral triangles in the homogeneous bulk of the computational domain;
and (ii) an unstructured mesh of triangles that conform to the external boundary.

3.2.1 Regular solution

We compute the lowest eigenvalue for the square cavity and Fig. 4 shows its
relative error for three different schemes: (i) circles – the proposed element; (ii)

triangles – the edge element [17] on triangles; and (iii) squares – the edge element [17] on squares with mass lumping by means of trapezoidal integration. Here, the dashed lines show results with uniform refinement of an unstructured mesh. The solid lines indicate the corresponding results for a grid of equilateral triangles as shown in Fig. 3.
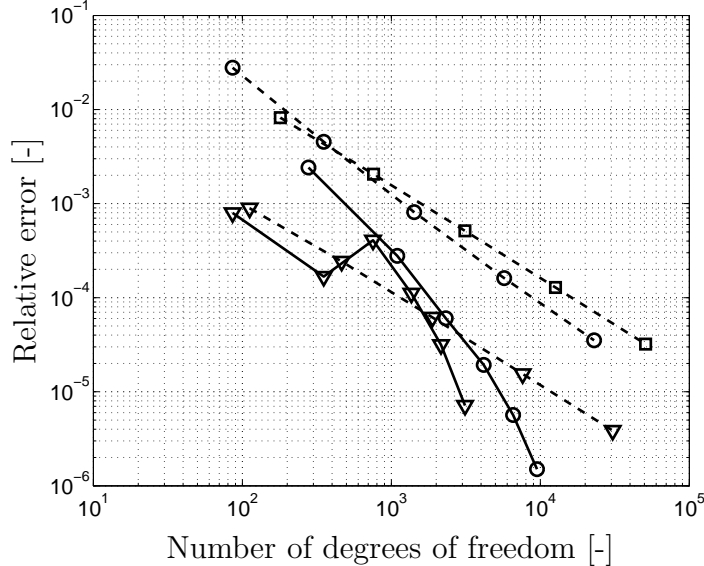
Fig. 4. Relative error of the lowest eigenvalue of a square cavity for three different schemes: (i) circles – proposed element; (ii) triangles – edge element on triangles; and (iii) squares – edge element on squares with mass lumping. Here, solid lines are used for meshes with equilateral triangles in the homogeneous bulk of the computational domain, and the dashed lines show results for uniform mesh refinement of an unstructured mesh.

Figure 5 shows the arithmetic average of the relative error for the ten lowest eigenvalues, as a function of the number of degrees of freedom. The squares show the result for the lowest order edge elements with mass lumping on a uniformly refined grid of squares. The triangles indicate the result for the lowest order edge element on triangles computed on a *non*-uniformly refined unstructured mesh – a case that has been identified to yield low errors due to cancellation effects [23]. The circles show the results for the proposed element on a mesh of the type shown in Fig. 3 with uniform refinement of the triangles in the bulk of the computational domain. It should be emphasized that the average error also contain contributions from eigenmodes that are not yet in the range of asymptotic convergence.

The number of non-zero elements in the stiffness matrix is approximately proportional to the computational cost associated with a matrix-vector multiplication that involves the stiffness matrix: (i) one such matrix-vector product is needed for each time step of an explicit method; and (ii) implicit time-integration methods that use conjugate gradients with some reasonable pre-conditioner typically need some 10-20 matrix-vector products to converge to

10
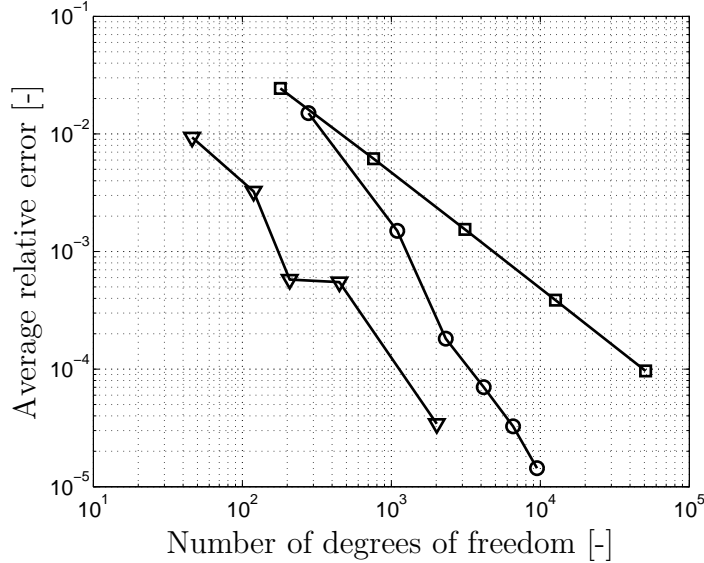
Fig. 5. Average relative error of the ten lowest eigenvalues of a square cavity for three different schemes: (i) circles – proposed element on mesh with mainly equilateral triangles; (ii) triangles – edge element on unstructured non-uniformly refined mesh of triangles; and (iii) squares – edge element on squares with mass lumping on grid with uniform refinement.

a tolerance that is comparable to a direct solver. Next, we consider the average relative error shown in Fig. 5 as a function of the number of non-zero elements in the stiffness matrix, instead of the number of degrees of freedom, and these results are shown in Fig. 6. As compared to the lumped edge elements on squares, the proposed element appears to be quite competitive when used with explicit time-integration. It should be noted that in the FDTD scheme spatial and temporal discretization errors cancel to some extent and such considerations are not taken into account here. However, the differences are sufficiently large to clearly show that the proposed element is competitive. The edge element on a triangular mesh yields a non-diagonal mass matrix and, thus, require about 10-20 matrix-vector products per time-step which makes the performance of such a method similar to the proposed method. It should be emphasized that, here, we assume that all the methods are operated with the same time step on similar meshes with uniform mesh size. For example, local mesh refinement reduces the global time-step of an explicit method and in such situations implicit time-stepping or hybrids [20] that combine explicit and implicit time-stepping typically are better.

3.2.2 Singular solution

Finally, we test the proposed element on an eigenvalue problem that features a sharp corner that supports a field singularity. Figure 7 shows the L-shaped computational domain, where we again use the boundary condition $\boldsymbol{n} \times \boldsymbol{E} = 0$. In particular, we emphasize that the proposed element does not show any signs

11
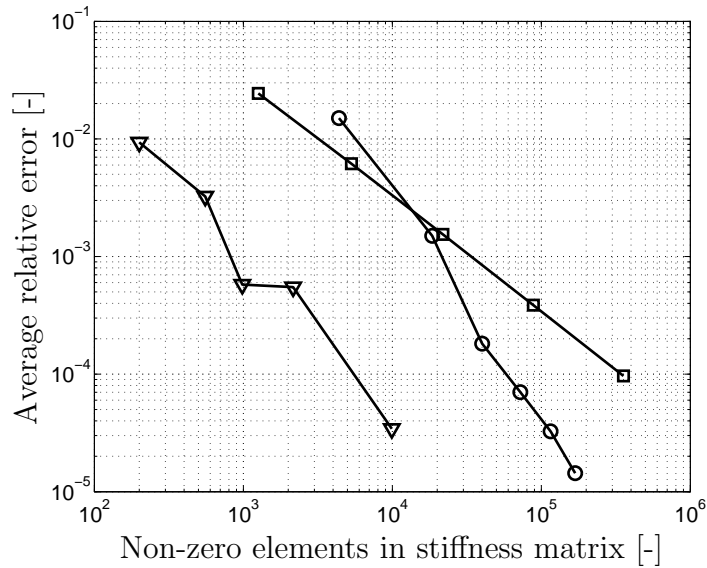
Fig. 6. Average relative error of the ten lowest eigenvalues of a square cavity for three different schemes: (i) circles – proposed element on mesh with mainly equilateral triangles; (ii) triangles – edge element on unstructured non-uniformly refined mesh of triangles; and (iii) squares – edge element on squares with mass lumping on grid with uniform refinement.

of generating spurious modes despite the presence of a singularity, and that the multiplicity of the lowest eigenvalues is correct. Here, we use a reference solution with six accurate digits computed by means of quadratic Lagrangian shape functions and adaptive mesh refinement.
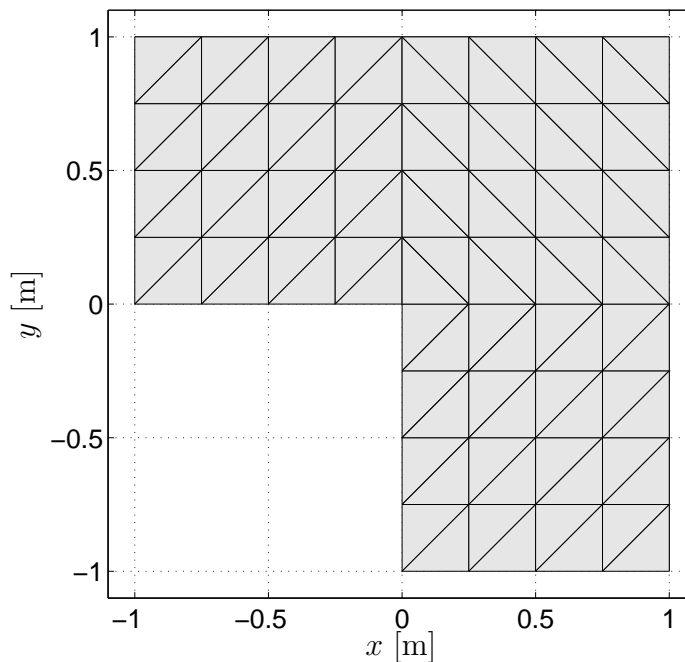
Fig. 7. Discretization of the L-shaped domain.

Figure 8 shows the relative error of the lowest eigenfrequency as a function of the number of degrees of freedom for a uniformly refined mesh of right-angled triangles: solid curve – the proposed element; and dashed curve – the conventional edge elements of the lowest order. It is clear that the relative error scales as $N^{-2/3} \propto h^{4/3}$. This is expected [1] for a PEC corner that subtends the angle $\alpha = \pi/2$, where the electric field in the vicinity of the corner scales as $r^{-1+\pi/(2\pi-\alpha)}$ with respect to the distance r to the corner. For the same number of degrees of freedom, the proposed element reduces the error by about a factor three as compared to the lowest order edge element. We attribute this to the ability of the proposed element to represent linear field variations exactly, which is useful in the immediate vicinity of the singularity. Clearly, the edge elements [18] that can represent complete linear fields would preform better as compared to its lowest order version [17].
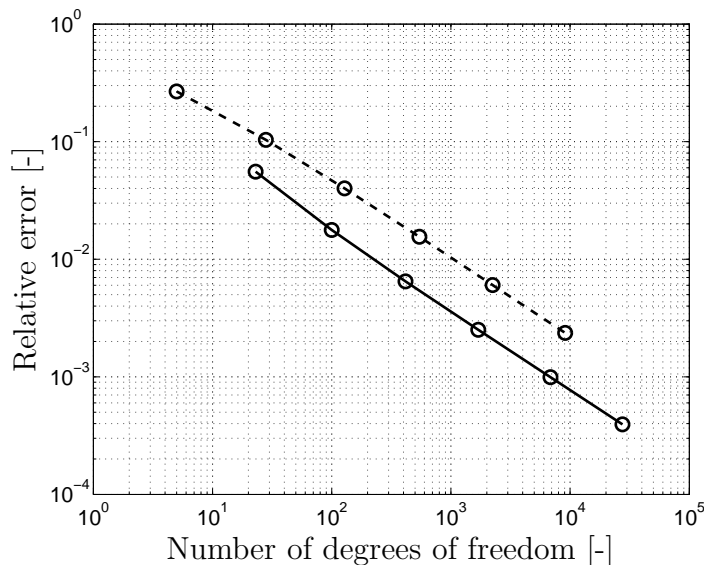
Fig. 8. Relative error for the lowest eigenvalue as a function of the number of degrees of freedom $N \propto 1/h^2$ for the L-shaped domain shown in Fig. 7: solid curve – proposed element; dashed curve – lowest order edge elements.

4 Conclusion

We have proposed a linear nonconforming finite element for Maxwell's equations formulated in two space dimensions. The element shape functions have degrees of freedom associated with the midpoints of the edges of the element. The tangential field at the midpoint of each edge is continuous, while the normal component is allowed to be discontinuous, yielding an approximation related to the Crouziex–Raviart element for Stokes. Our formulation features a parameter γ that stabilizes the tangential continuity at element edges, which allows for tuning aimed at improving the accuracy of the method.

13

We conclude that the proposed element yields a discretization error that is proportional to the square of the mesh size for problems with smooth boundaries, which is expected since it can model linear field variations exactly. A numerical dispersion analysis on a periodic grid shows that the proposed element yields second order convergence towards the analytical dispersion relation. For the case with stabilization, we find four branches with $\omega(\boldsymbol{k}) = 0$ that correspond to modes with an irrotational electric field that can be expressed as the gradient of a scalar potential: (i) one linear Lagrangian basis function ϕ_i associated with the node of the unit cell; and (ii) three edge-bubble basis functions $\phi_i\phi_j$ associated with the three edges of the unit cell. (The case without stabilization yields an additional three branches with $\omega(\boldsymbol{k}) = 0$.) The lowest non-zero branch $\omega(\boldsymbol{k})$ correspond to the physical dispersion relation and it shows a relative error that is proportional to $(h_T k)^2$, where h_T denotes the maximum edge length of the mesh. The remaining non-zero branches yield very large values for $\omega(\boldsymbol{k})$, which makes them easy to identify and disregard. We find that it is feasible to optimize the stabilization parameter γ on a periodic grid of equilateral triangles in order to achieve very low errors in the dispersion relation for large regions in $\boldsymbol{k}$-space.

Eigenvalue analysis of a square shaped cavity reinforces the convergence properties found in the dispersion analysis. In addition, we find that the accuracy of the proposed element is rather good with respect to the number of non-zero elements in the stiffness matrix, when it is compared to the lumped edge elements on rectangles that are used for the spatial discretization in the popular finite-difference time-domain (FDTD) scheme. We emphasize that the proposed element does not suffer from spurious solutions and that it reproduces the well-resolved eigenvalues with the correct multiplicity, also for problems where the field solution is singular. Finally, we conclude that the proposed element allows for explicit time-stepping and yields accurate and robust results. These characteristic features makes our element very suitable for computationally challenging electromagnetic field problems that feature complex geometry, e.g. large conformal array antennas.

Acknowledgments

References

[1] A. Bondeson, T. Rylander, P. Ingelström, Computational Electromagnetics, Springer, Berlin, 2005.

[2] S. C. Brenner, F. Li, L. Y. Sung, A locally divergence-free nonconforming finite element method for the time-harmonic Maxwell equations, Math. Comp. 76 (2007) 573–595.

[3] S. C. Brenner, J. Cui, F. Li, L. Y. Sung, A nonconforming finite element method for a two-dimensional curl–curl and grad–div problem, Numer. Math. 109 (2008) 509–533.

[4] A. Buffa, P. Houston, I. Perugia, Discontinuous Galerkin computation of the Maxwell eigenvalues on simplicial meshes, J. Comput. Appl. Math. 204 (2007) 317–333.

[5] A. Buffa, I. Perugia, Discontinuous Galerkin approximation of the Maxwell eigenproblem, SIAM J. Numer. Anal. 44 (2006) 2198–2226.

[6] E. Burman, P. Hansbo, A stabilized non-conforming finite element method for incompressible flow, Comput. Methods Appl. Mech. Engrg. 195 (2006) 2881-2899.

[7] G. Cohen, Higher Order Numerical Methods for Transient Wave Equations. Springer, Berlin, 2002.

[8] M. Crouzeix, P. A. Raviart, Conforming and nonconforming finite element methods for solving the stationary Stokes equations, RAIRO Sér. Rouge 7 (1973) 33–75.

[9] D. Degerfeldt, T. Rylander, A brick-tetrahedron finite-element interface with stable hybrid explicit-implicit time-stepping for Maxwell's equations, J. Comput. Phys. 220 (2006) 383–393.

[10] A. Elmkies, P. Joly, Éléments finis d'arête et condensation de masse pour les équations de Maxwell: le cas 2D, C. R. Acad. Sci. Paris, Ser. I 324 (1997) 1287–1293.

[11] P. Hansbo, M. G. Larson, Discontinuous Galerkin and the Crouzeix-Raviart element: Application to elasticity, ESAIM: Math. Model. Numer. Anal. 37 (2003) 63–72.

[12] Y. Haugazeau, P. Lacoste, Condensation de la matrice masse pour les éléments finis mixtes de H(rot), C. R. Acad. Sci. Paris, Ser. I 316 (1993) 509–512.

[13] J. S. Hesthaven and T. Warburton, High-order accurate methods for time-domain electromagnetics, Comput. Model. Eng. Sci. 5 (2004) 395–407.

[14] P. Lacoste, La condensation de la matrice masse, ou mass-lumping, pour les éléments finis mixtes de Raviart-Thomas-Nédélec d'ordre 1, C. R. Math. Acad. Sci. Paris 339 (2004) 727–732.

[15] P. Monk, Finite element methods for Maxwell's equations, Oxford University Press, New York, 2003.

[16] P.B. Monk, A.K. Parrot, A dispersion analysis of finite element methods for Maxwell's equations, SIAM J. Sci. Comput., 15 (1994) 916-937.

[17] J. C. Nédélec, Mixed finite elements in $\mathbb{R}^3$, Numer. Math. 35 (1980) 315–341.

[18] J. C. Nédélec, A new family of mixed finite elements in $\mathbb{R}^3$, Numer. Math. 50 (1986) 57–81.

[19] I. Perugia, D. Schötzau, P. Monk, Stabilized interior penalty methods for the time–harmonic Maxwell equations, Comput. Methods. Appl. Mech. Engrg. 91, (2002) 4675–4697.

[20] T. Rylander, A. Bondeson, Stability of explicit-implicit hybrid time-stepping schemes for Maxwell's equations, J. Comput. Phys. 179 (2002) 426–438.

[21] A. Taflove, S. C. Hagness, Computational Electrodynamics: The Finite-Difference Time-Domain Method (3rd Ed.), Artech House, Boston, 2005.

[22] T. Warburton, M. Embree, The role of the penalty in the local discontinuous Galerkin method for Maxwell's eigenvalue problem, Comput. Methods Appl. Mech. Engrg. 195 (2006) 3205–3223.

[23] J.-Y. Wu, R. Lee, The advantages of triangular and tetrahedral edge elements for electromagnetic modeling with the finite-element method, IEEE Trans. Antennas Propagat. 45 (1997) 1431–1437.

[24] K. S. Yee, Numerical solution of initial boundary value problems involving Maxwell's equations in isotropic media, IEEE Trans. Antennas Propagat. AP-14 (1966) 302–307.